CONFERENCE PAPER

In-Vitro Mechanical Characterization of Scaffolds for Bone Regeneration Obtained by Sterolithograpy

Madeline H. Jeffery
Department of Mechanical Engineering, Institute for Research in Technology, Universidad Pontificia Comillas, Alberto Aguilera 25, 28015 Madrid, Spain
College of Engineering, University of Michigan, 500 S State St, 48109 Ann Arbor, MI, USA

Abstract
The medical standard for skeletal fracture treatment has historically been through the use of autografts and allografts. Limitations involving donor availability and increased risks of infection, however, have caused the field of orthopedics to investigate alternatives such as biocompatible scaffolding produced through stereolithography. This study's objective was to characterize the mechanical properties of a biocompatible resin, BioMed Clear, for future use in scaffolding for patients with bone damage. Two samples of BioMed were printed: a porous sample set and a bulk sample set. The porous samples had intricate microstructures similar to those of cancellous bones whereas the bulk samples had compact, solid microstructures which imitate cortical bones. Each sample set underwent aging in a Phosphate Buffered Saline (PBS) for up to thirty days. This process mimics the aging that BioMed will experience after long periods of time within the body. One of four tests was then performed on the specimen—a bending, single-edged notched bending (SENB), compression, or Charpy impact test. Each test served to simulate the conditions of the human body at different times and at different points of stress. This study found that after longer periods of aging, the elastic properties of BioMed decreased while the energy density slightly increased; this was true for both sample types. These trends signify that, over time, BioMed will likely deteriorate within the body. Research on BioMed is ongoing with additional experiments being conducted on samples aged for thirty to ninety days to better understand the material's behavior over extended periods of time.

Keywords: Bone-Tissue Engineering, Bone Graft, Scaffold, Bone Regeneration

---

1. Introduction
Bone grafts are used to promote bone healing and stimulate osseon growth in cases involving the implantation of a surgical device, multiple or complex skeletal fractures, bone fusion across a diseased joint, or bone loss resulting from disease, infection, or injury. Approximately 2.2

million bone grafts are used in medical procedures worldwide each year, attesting to the high frequency of these health conditions as well as the popularity of bone grafting[1]. There exist two types of bone grafts: autografts, which use bone from one's own body, and allografts, where the bone is harvested from a donor. Autografts are considered to be the medical standard as it does not bring into question donor availability and the risk of immune rejection is nonexistent. There are drawbacks, however, as this surgery necessitates the removal of bone from an otherwise healthy part of the body and as such the possibility of pain, scarring, and surgical complications are much higher. To mitigate these concerns and shift away from auto and allografting, researchers have been investigating a new alternative that would facilitate bone regeneration while lessening the inherent risks associated with bone grafting.

Biocompatible bone scaffolding aims to produce a biocompatible material that would stimulate bone regeneration through the attachment and multiplication of osteo inducible cells on its surfaces. Current research has determined that while no perfect sample has yet to be fabricated, a collagen scaffold of either a porous or bulk structure—depending on the scaffold's purpose in regenerating cancellous or cortical bone—is most suitable for biocompatible bone scaffolding[2]. There are multiple factors to take into consideration for this strategy: 1) the scaffold architecture which must mimic the surrounding bone structure while providing ample surface area to support bone growth, 2) the mechanical properties of the biocompatible material that will need to withstand the conditions of the human body during daily activity, and 3) the biodegradability that will allow for the substitution of the biocompatible scaffolding with the regenerated bone. This research study primarily focuses on the second item of the aforementioned strategy considerations—the mechanical characterization of a newly developed biocompatible resin, BioMed Clear (BioMed). Stereolithography was used to print this BioMed resin into various samples necessary for testing. Prior research indicated that the incorporation of select additives into 3D printing resins had been shown to improve the strength and quality of certain prints[3]. To investigate this phenomenon and its potential for future BioMed scaffolds, strengthening composites were added to a general purpose clear resin before it was printed and tested.

2. Materials and Methods

To achieve a complete understanding of BioMed and its capabilities as a potential scaffolding material, the research process involved three key parts: stereolithography, testing, and data analysis. Each of these processes are described in detail below.

2.1 Stereolithography (SLA)

Additive manufacturing was used for the production of all resin samples incorporated in later testing. To prepare the three variations of resin mixtures, a variety of laboratory equipment was utilized, including a desiccator complete with silica gels, a mechanical stirrer, an Elma Ultrasonic Cleaner, an oven, a multitude of common laboratory items, methyl methacrylate (MMA), and nanostrength materials that were added into the resin which was aged in Phosphate

Buffered Saline (PBS). The printing equipment included a Formlabs Form 2 3D printer alongside Form Wash and Form Cure post processing containers. The testing involved calipers for measurements as well as an Instron CEAST 9050 device[4] and an Ibertest IBTH Monotrac 5-500 testing stand[5].

(1) Resin Preparation

Three resin variations were produced and used within lab tests. The first sample material, "Clear," was a general purpose 3D printing resin manufactured by Formlabs. Its fast printing speed, high accuracy, and strong mechanical properties made it an ideal choice to be used as a baseline for comparison in later experiments[6].

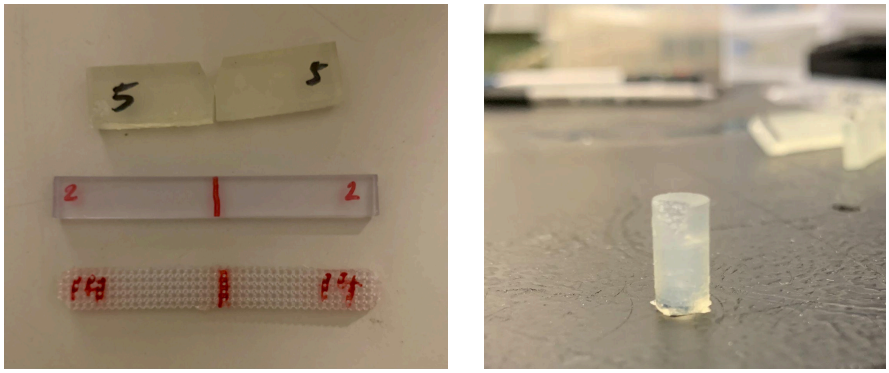
The second specimen, "Clear + NS" or "Strengthened," introduced a mixture of nanostrength and methyl methacrylate (MMA) to the baseline clear resin. To create this modified resin, the mixture required 300mL of Clear measured by scale; 20mL of MMA extracted by way of adjustable volume pipette; and 5% nanostrength weight by volume of Clear which was likewise weighed by scale. The MMA was then combined with 150mL of the Clear resin in a mechanical stirrer for 3 minutes at 350 rpm to fully incorporate the MMA into the resin. Next, the nanostrength was added to the mixture which was stirred in the mechanical stirrer for five minutes at 600 rpm; the stirring speed and time were increased due to the high viscosity of the mixture. After adding the remaining resin to this mixture, it was again stirred for five minutes at 900 rpm, creating a homogenous mixture. The batch was then placed in the Elma Ultrasonic Cleaner for 15 minutes to remove air bubbles which, if unaddressed, would cause defects in the printed samples. The final step before the mixture was completed was to place the resin into the oven at 39℃ for 15 minutes for cooling. Because the resin had the tendency to overflow, the oven had to occasionally be depressurized to prevent the resin from spilling over. It is important to note that two versions of this resin type were created: one in which the nanostrength was added without modifications and one in which it was dried before its addition. The only difference being that the second was dried for 24 hours with moisture-absorbing silica gels.

The final resin material type, BioMed, was a transparent, wear-resistant resin suitable for biocompatible applications. Prior to testing, this material underwent aging in PBS for 1, 7, or 30 days. Current research suggests that though PBS maintains tissue hydration, there are negative effects in long-term mechanical tests; thus, samples were immersed in PBS and aged in a 60℃ oven to investigate the effects of aging on BioMed's mechanical properties[7]. Additional aging is expected to be completed for 90 and 180 days which was not possible in the duration of this research study due to time constraints.

(2) Sample Types

Three sample designs were printed and used in one of four mechanical tests so as to properly evaluate BioMed's mechanical properties. Samples were thus designed to fit a test's

specifications and were designated with a corresponding name; there is a single-edged notched bending (SENB) sample model, a bending/charpy sample model, and a compression sample model. Of these three designs, only the bending/charpy model—a long rectangular sample piece—could be fabricated with either a bulk or porous microstructure. The bulk build resembles a cortical bone and its compact, solid microstructure while the porous build imitates a cancellous bone with its lighter and extensive lattice matrix. Due to testing requirements, the SENB and compression samples could not be printed with a porous microstructure and instead featured the bulk build. Each of the three models and the two structure designs can be seen below in Fig. 1.



(a) (b)

Figure 1. Four sample variations produced through stereolithography. Figure 1(a) depicts the SENB (uppermost) and bending/charpy (bottom two) samples. The yellowed coloring of the SENB sample is a result of aging in the PBS solution. The lowermost sample in Fig. 1(a) is a bending/charpy sample featuring a porous build while the middle sample in Fig. 1(a) features a bulk build. A compression sample can be seen in Fig. 1(b). It is important to note the defect towards the upper left hand side of the sample created during the printing process. This defect likely resulted from overcrowding on the printing tray.

The SENB sample was manufactured with the strengthened resin and with the BioMed resin, both with a bulk build. Due to the type of testing, a porous build was not possible. The design plans for this sample are depicted below in Fig. 2.

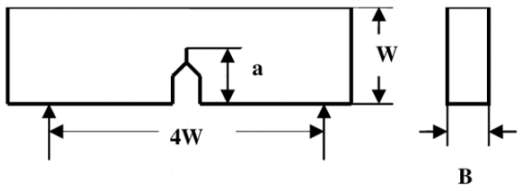


Figure 2: Front and side views of SENB sample. The design value is 14mm for *W* and 7mm for *B*. Due to the high accuracy of the printer, these dimensions saw low values of deviation. The notch in the sample was machined during post processing and likewise saw little deviation from its design value of 7mm.

While the SENB samples could only be printed with a bulk build, certain prints of the bending/charpy samples could be manufactured with either a bulk or a porous structure, depending on the material type. The bending/charpy sample was printed in each of the three resin options: Clear, Strengthened, and BioMed. Only the BioMed bending/charpy samples had the opportunity to be printed with a porous structure as the Clear and Strengthened resins had high viscosities which prevented a clean print. The target dimensions for a bending/charpy sample

were 4mm x 10mm x 80mm but, due to shrinkage, the actual dimensions were subject to change.

The final sample type, compression, is pictured on the right in Fig. 1(b). The compression samples were fabricated with either the Clear or Strengthened resins and were structured only with the bulk design as the porous build was not suitable for this testing type. BioMed was not used as a material for the compression testing samples due to time constraints. The compression samples aimed to measure 6mm in diameter and 12mm in height. A summary table of each sample type's dimensions, materials, and builds has been provided within Appendix A.

(3) Printing and Post Processing

Following the successful preparation of the resin, the samples were printed in batches with a Formlabs Form 2 3D printer; the number of samples printed varied in accordance with the week's demands and the duration of printing lasted between 5 and 6 hours. Once the samples were printed and disconnected from their support structures, they were washed in a Form Wash device and cured in a Form Cure machine. Pictures of these post processing instruments are depicted in Fig. 3, below.



(a) (b) (c)

Figure 3. Shown above is the Formlabs Form 2 3D printer (a), the Formlabs Form Wash (b), and the Formlabs Form Cure (c). These photographs were provided courtesy of Formlabs[8].

The Form Wash machine opened at the top and contained a basket in which the samples were placed; there, they were washed in isopropanol for 20 minutes to remove the residual resin. Following the washing process, any remaining support structures were removed and the samples faced the hour-long curing process. Samples were placed upright in the Form Cure device which hinged open at the front. The curing process preserved the sample's maximum mechanical properties and ensured dimensional accuracy. After 60 minutes at 60℃, the samples were removed and patted dry. The majority of the samples were then ready for testing; the SENB, compression, and porous prints required further post processing. A razor blade was used to create a pre-crack in the machined notch in the SENB sample. It passed through the notch twice and was retired after cutting 12 specimens, ensuring a sharp blade was used for each SENB sample.

The compression samples were sanded with grit paper on their flat edges to be parallel with one another; errors in printing caused unevenness which had large ramifications if unaddressed. The porous samples were blown with compressed air before testing to rid any excess material. Once these steps were completed, all samples were properly readied for testing or aging.

Only the BioMed samples were aged as the effects of aging on the clear resins were not within the scope of this research project. The post processed BioMed prints selected for aging were immersed in PBS and sealed in a 200 mL container. The containers were placed in a 60℃ oven for the duration of the aging process — 1, 7, or 30 days. Once the aging process was complete, the samples were removed from the PBS and patted dry, now ready for testing.

2.2 Testing

Four different tests were performed on the samples: SENB, three point bending, charpy, and compression testing. Each test was repeated with each material no fewer than five times so as to reduce precision error. Prior to the start of testing, the samples were labeled and their dimensions measured with calipers. Their centerlines were marked and used to align the samples on the testing machines. Two testing devices were used: an Instron CEAST was used for the charpy test as well as an Ibertest IBTH Monotrac 5-500 that was operated in conjunction with WinTest software and utilized for the remaining tests. The IBTH could be customized with different attachments for various tests. Each of these tests are described in further detail, below.

(1) SENB

To begin the SENB testing, the IBTH was outfitted with the three point bending attachment; one point pushed onto the center of the SENB sample and the other two points supported the sample at a distance of 56mm or quadruple the width. This was in accordance with IPC testing standards[9]. Once at the appropriate distance, the SENB sample was placed crack side down with its center aligning with the pushing prong. A picture of this setup can be seen below in Fig. 4.

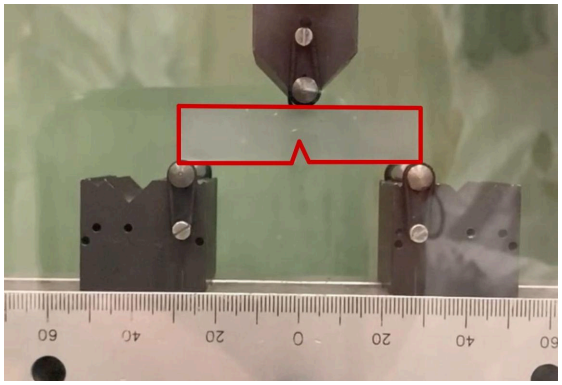


Figure 4. SENB testing setup. The SENB sample is outlined in red for clarity. Note that the notch in the sample is facing downwards. This is to ensure the sample fractures rather than simply bends. Measured by the point of contact between the support and the sample, the two lower prongs are placed a distance of 28mm away from the centerline or 56mm total. To achieve the correct distance, hex keys were used to adjust the two bottom prongs in accordance with the affixed ruler. The third prong pushes down in the center of the SENB sample with increasing weight at a set speed of 10mm/min. All testing procedures are in accordance with the IPC testing standards[6].

Once secured in the IBTH machine, the push prong applied a downwards force on the SENB sample until it achieved complete fracture. A transparent cage surrounded the IBTH machine and protected researchers from potential flying shards resulting from fractured samples; the enclosure also served to contain the experiment. The WinTest software collected data from the experiment, including the time, force, and displacement of the experiment. This information made it possible to complete later calculations on the sample's material properties.

(2) Three Point Bending

The IBTH Monotrac apparatus was also used to conduct the three point bending testing. The two supporting prongs were moved a distance of 60mm apart, following ISO guidelines[10]. The speed was reduced to 5 mm/min to allow for gradual bending rather than clear fracture. A depiction of the three point bending setup can be seen in Fig. 5.

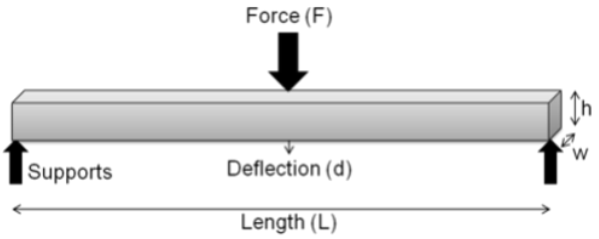


Figure 5. Three point bending model setup. The testing is similar to that of the SENB with the three prongs but the wider base and slower speed test the material's elastic bending instead of its fracture point.

The experiment was conducted until the WinTest software displayed a decrease in the force applied to the sample or until the sample began to support itself on the sides of the prongs. Due to the high levels of force applied to the elastic sample, it was possible for the specimen to flex to the point where it was no longer supported by the rounded point of the prong but rather by the inner edge of the prong's base. Once the sample reached this point, the experiment was stopped and the data collected. Analysis was then conducted on the sample's mechanical performance.

(3) Charpy

The charpy test utilized the Instron CEAST with a small hammer attachment. This ensured a low energy configuration which was necessary for the test type. To begin testing, the hammer was knocked in the upright position with the sample placed in the blocks below. A thin metallic lever pivoted upwards from the base of the machine and aligned with the stops. Prior to testing, this lever was lifted vertically upwards to ensure the sample was centered in the machine. When the hammer was released, it swung downwards on a pendulum and shattered the sample while the machine collected energy loss data. The final piece of the machine was the transparent cage which, much like the IBTH device, surrounded the pendulum and served to shield researchers. Figure 6 details the full setup of this test.

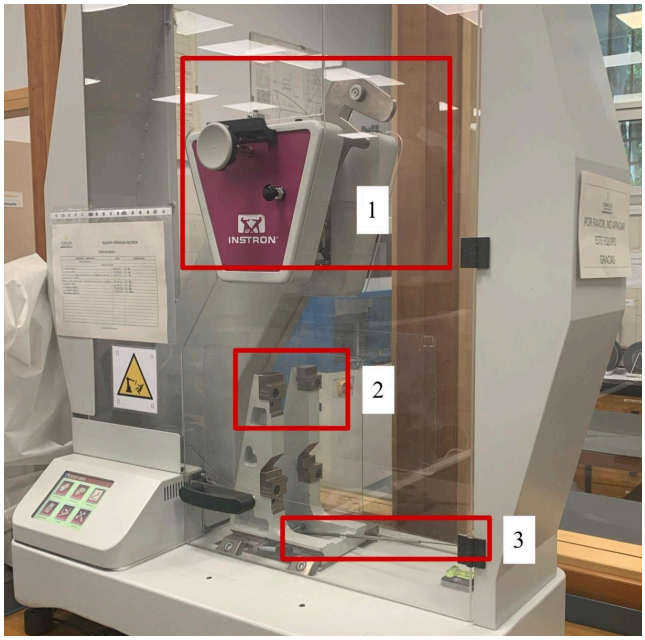


Figure 6. Instron CEAST 9050 charpy testing setup with key parts outlined in red for clarity. In box 1 lies the pendulum controls and hammer. Pulling the black button in the lower left quadrant of the box nocks the hammer in the upright position. The large gray stop at the left of box 1 is the pendulum brake, pulled following the completion of the experiment. The stops at which the sample is placed can be seen in box 2. Box 3 shows the lever centering device used to ensure the sample is aligned properly. The screen in the lower left corner of the testing machine displayed the data collected during experimentation.

Prior to each round of testing, the machine was calibrated to account for normal energy loss during the pendulum motion. The pendulum was released without a sample in place and swung freely. With the smaller, lower energy hammer attachment, an average of 4J of energy was lost.

(4) Compression

The compression testing again used the IBTH Monotrac but with the parallel plates fixture. The samples were placed in the center of two concentric plates, the upper of which lowered at a speed of 20 mm/min to compress the sample. Figure 7, below, depicts this setup.

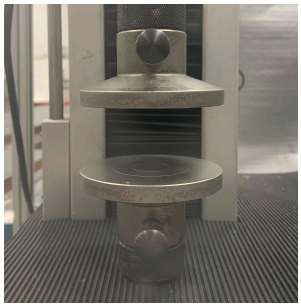


Figure 7. Compression testing setup. Note the bolts affixing the upper and lower plates. Removing these bolts allowed the IBTH to be customized with different attachments for each of the different tests.

Special care was taken to observe the samples during experimentation and ensure they were properly compressed. As previously described, the compression samples were sanded before testing to reduce error in testing. Due to variations in printing, the cylindrical compression samples were not consistently level. Before addressed, this led to large errors during testing from the parallel plates as the force would not be evenly distributed throughout the sample. Visually, this was seen as the samples would compress and bulge on one side, shattering prematurely. To prevent this, samples were sanded with grit paper and closely watched during compression. If the samples bulged disproportionately, the results were marked as outliers and voided.

2.3 Calculations and Graphing

Each of the four tests on the various resins evaluated a minimum of one material property. The SENB test determined the fracture toughness, K_{IC}; the bending test studied the flexural toughness, σ_F, and Young's Modulus, E; the charpy test measured energy density; and the compression test assessed the Ultimate Tensile Strength, UTS, Young's Modulus, and maximum force achieved during testing, F_{max}. The calculation for the fracture toughness can be seen below in Eq. (1).

$$K_{IC} = \frac{P_Q L}{BW^{3/2}} f\left(\frac{a}{W}\right) \quad (1)$$

In this equation, L represents the length of the sample, B represents the thickness of the sample, W represents the width of the sample, and a represents the crack length; these dimensions are outlined in Fig. 2. The function $f(\frac{a}{W})$ relates the crack length to the width and can be found in Appendix B. The value of P_Q is found graphically using a plot of the schematic load (P) against the crack-mouth opening displacement (Δ). A line whose slope is five percent of the original slope of the P-Δ curve is projected against said P-Δ curve; the intersection is thus P_Q or, if the curve has a maximum before that point, P_Q will be the maximum of the curve. An in-depth guide to this process is provided in Appendix C.

With the bending test, two material properties were calculated: the flexural stress and Young's Modulus. The flexural stress is a measure of the maximum stress the material can withstand before failure. It is calculated with Eq. (2), below.

$$\sigma_F = \frac{3PL}{2WH^2} \quad (2)$$

The variables in this equation signify the same as those in Eq. (1) with H representing sample height. Using the flexural stress values calculated with Eq. (2), the second property determined by bending testing—the Young's Modulus—could be calculated. Two graphs were created and

evaluated to determine this value. The first graph used collected data to model the flexural stress against the flexural strain. Flexural strain, ε_F, can be calculated with Eq. (3).

$$\varepsilon_F = \frac{6\delta H}{L^2} \tag{3}$$

Material displacement, δ, is the only new variable in this equation. With both the flexural stress and flexural strain, it was possible to model a stress-strain curve. Using this graph, the initial slope was isolated and later mirrored on a second graph. From this second graph, it was easy to determine whether the slope was straight or curved. If the slope bended, different data points were selected and the slope reevaluated until it was consistent. Once achieved, this value was determined to be the corresponding sample's Young's Modulus. Appendix D depicts this process.

Compression testing likewise measured the Young's Modulus using this same method of dividing and averaging the material's stress by its strain during the initial testing period. In addition to evaluating the Young's Modulus, the compression tests calculated the Ultimate Tensile Strength. The UTS was calculated with Eq. (4), below.

$$UTS = \frac{P}{A} = \frac{4P}{\pi D^2} \tag{4}$$

This equation utilizes similar variables as in earlier formulas. Here, P symbolizes the maximum force achieved during testing while A represents the sample's area and D signifies the sample's diameter. With this equation, all desired material properties had been accounted for. No calculations were performed using the charpy data; the machine output the needed figures regarding energy density, U.

3. Results

The testing results have been divided by resin type into two sections: Clear and Strengthened data and Aged Biomed data. WinTest software was used during data collection and Universidad Pontificia Comillas proprietary software was used for data analysis. The data presented in this section are the mean averages of several tested samples and are presented alongside their respective standard deviations. This precision error dominated and as such, the resolution error in the calipers, accuracy errors in the 3D printer and testing machines, and any other additional errors were not taken into consideration. All results are summarized below and include relevant tabulated data and graphed patterns.

3.1 Clear and Strengthened Data

As aforementioned, two main forms of the clear resin existed: the Clear resin, which contained no additives, and the Strengthened resin, which included MMA and nanostrength into the resin mixture. The Strengthened resin, itself, had two variations of the same formula. In one batch, the

nanostrength was added as-is and without additional processing while a second batch saw the nanostrength dried before incorporation into the resin; in later tables, this distinction is made by labeling the dried nanostrength samples "Clear + MMA + dNS". All results for the Clear and Strengthened samples alongside their respective errors are given below in Table 1.

Table 1. Average material properties of Clear and Strengthened data with associated error. Cells left blank were neither printed nor tested in the related material and sample type.

	SENB	**Compression**		**Charpy**		**Bending**	
Resin Type	K_{IC} $(MPa\sqrt{m})$	$UTS\ (MPa)$	$E\ (GPa)$	$F_{max}\ (kN)$	$U\ (KJ/m^2)$	$E\ (GPa)$	$\sigma_F\ (MPa)$
Clear	-	0.34 ± 0.04	1.7 ± 0.1	9.6 ± 1.3	10.1 ± 2.6	0.8 ± 0.1	39.6 ± 0.5
Clear + MMA + NS	-	0.30 ± 0.05	1.6 ± 0.1	8.7 ± 1.5	7.4 ± 0.3	-	-
Clear + MMA + dNS	2.1 ± 0.2	0.11 ± 0.02	0.7 ± 0.1	3.2 ± 0.7	17.3 ± 6.6	0.8 ± 0.1	86.6 ± 1.9

The variable F_{max} is a measure of the maximum force that a sample withstood before complete compression; its value was recorded by software during testing. The missing data in the Clear + MMA + NS bending samples resulted from human error during testing; the three point bridge was not adjusted to the appropriate distance and thus the collected data was invalid. Time constraints prevented retesting. SENB testing likewise saw gaps in its data as a result of the prioritization of the compression, charpy, and bending tests.

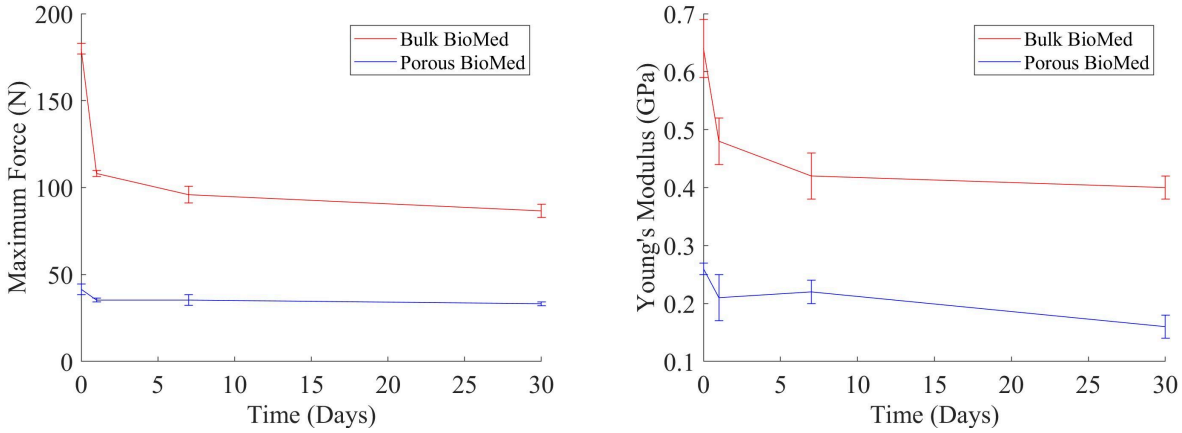
3.2 Aged BioMed Data

All three tests conducted with aged BioMed—SENB, bending, and charpy—saw noticeable variations in their material properties with regard to time spent aging. Averages from the SENB testings can be seen below in Table 2.

Table 2. Average fracture toughness of SENB samples following aging for various time periods.

	Duration of Aging (Days)			
	0	1	7	30
Fracture Toughness $(MPa\sqrt{m})$	1.18 ± 0.09	1.05 ± 0.10	0.49 ± 0.03	0.51 ± 0.03

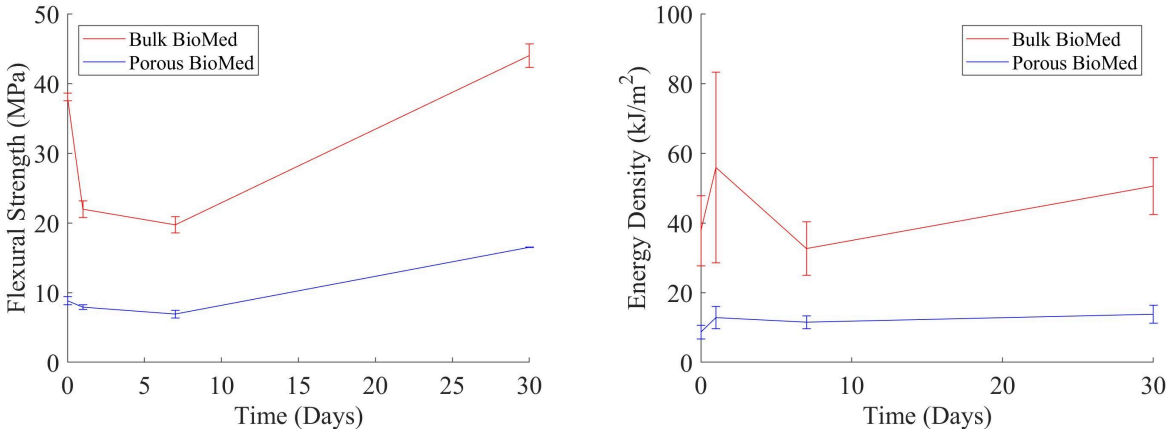
SENB samples saw fracture toughness decrease proportionally with age before plateauing at $0.5\ MPa\sqrt{m}$. The bending tests saw similar results in two of its tested mechanical properties: the maximum force withstood by each sample and the Young's Modulus performance. Each experienced an eventual plateau as aging duration increased. Figure 8, below, shows this trend. Note that these graphs were created using data from both bulk and porous BioMed bending tests.



(a) (b)

Figure 8. Plots of Maximum Force vs Time (a) and Young's Modulus (*E*) vs Time (b). For the Max. Force, the bulk BioMed plateaued at 87 N and the porous BioMed plateaued at 33 N. For *E*, the bulk BioMed plateaued at 0.4 GPa while the porous BioMed continued to decline after the 30 days. There was no error overlap between any data point; the bulk samples consistently achieved higher material properties.

The bending and charpy tests experienced decidedly different results. Rather than plateauing, the samples saw a drop in their mechanical properties with initial aging before a gradual rise after prolonged exposure. The results for porous and bulk samples yielded similar data patterns, as seen below in Fig. 9, which models the trends for the bending and charpy samples.



(a) (b)

Figure 9. Plots of Bending (a) and Charpy (b) BioMed material properties—flexural strength and energy density, respectively—as they evolve with aging. The flexural strength fell to 19.72 MPa for the bulk BioMed and 6.92 MPa for the porous BioMed; both samples achieved their lowest values after seven days before rising again. Note the large error bars in the Charpy one day aged testing. This was due to outliers in the data that, when removed, left gaps in the data. Despite the large error, there was no overlap between the bulk and porous results, meaning that the bulk resin is definitively the more energy dense material.

Both bulk and porous bending samples reached their lowest flexural strength values after one week. Their mechanical properties then rose after 30 days to be higher than their original values. Likewise, the bulk and porous charpy tests saw similar data patterns in their energy densities. Both reached a relative peak after day 1, followed by a decline lasting through day 7, and, finally, a gradual rise until day 30. The bulk BioMed, however, had a more dramatic behavior, peaking at 55.9 kJ/m^2 compared to the porous BioMed's 12.8 kJ/m^2. Excluding the SENB results, the bulk BioMed samples demonstrated higher mechanical properties compared to its porous counterparts in each test, likely due to its compact build.

4. Discussion and Conclusion

From the results of each experiment, it is clear that though BioMed is not the ideal material for a biocompatible scaffold, more testing will be necessary to identify any ideal additives and ideal aging trends. Of the Clear resin experimentation, only the results for the compression tests were complete; the remaining tests were not performed on each of the Clear resin variations—Clear, Clear + MMA + NS, and Clear + MMA + dNS. Testing on the BioMed resin, meanwhile, was performed at each time interval and on each of the build types; the BioMed testing was fully completed.

The results of the Clear experiments were counterintuitive. Prior to testing, it was expected that with the strengthening materials, the material properties would grow stronger. That, however, was not the case as the addition of MMA and nanostrength saw the samples' material properties decrease in strength rather than increase. The maximum force achieved during the compression tests fell from 9.6 ± 1.3 for the Clear resin to 8.7 ± 1.5 for the Clear + MMA + NS resin to 3.2 ± 0.7 for the Clear + MMA + dNS resin. Expectations were that with the strengthening materials, more force would be necessary to compress the samples as the resin would be stronger. Similarly, the ultimate tensile stress and bending modulus decreased with the addition of the MMA and nanostrength; the dried nanostrength saw a greater decline in these material properties. Further experimentation should be conducted to better understand this behavior. Due to the unexpected performance of the strengthening materials, the incorporation of MMA and nanostrength into the BioMed should be avoided until an explanation can be identified.

The aged BioMed resin behaved expectedly. With longer periods of aging, it was determined that the material properties of the BioMed resin weakened. The fracture toughness halved after a period of thirty days and plateaued around 50 $MPa\sqrt{m}$. Ideally, the fracture toughness would be higher—closer to that of the respective cortical or cancellous bone—as the biocompatible scaffolding is meant to be used in conjunction with an active human body. The results from the bending tests were similarly disappointing; this was true for both the bulk and porous samples. The bulk BioMed material experienced higher material properties compared to the porous build. This was expected as the difference in structures purposefully mimicked the differences between cortical and cancellous bones; cortical bones are naturally stronger and stiffer than cancellous

bones. Though the bulk and porous samples achieved numerically different results, they shared similar data patterns. The Young's Modulus and maximum force withstood likewise experienced unsatisfactory results: their material properties sharply decreased after a day of aging before they plateaued at a value below what is ideal for bone scaffolding. A biocompatible scaffolding material should be able to withstand the stresses a body experiences in day-to-day life. Therefore, the scaffold should more closely mirror the material properties of the bone it is mimicking, whether it be cortical or cancellous. Two of the BioMed samples' material properties increased with aging: flexural strength and energy density. In other words, after aging, the sample was more resistant to bending and required more energy to be fractured. These results were expected and agreed with prior research regarding the relationship between flexural strength and aging as well as energy density and aging[11]. Though the behavior of the aged BioMed was properly predicted, the mechanical properties devolved to levels that are not suitable for a biocompatible bone scaffold.

It is important to note that at the conclusion of this research project, the research was left incomplete. Further testing needs to be conducted on the Clear resin variations, assuring that each variation is properly tested with each of the SENB, Charpy, Compression, and Bending tests. The MMA and nanostrength additives likewise need to be further investigated as their inclusion into the Clear resin saw a steep drop in the material properties rather than the expected strengthening of them. Additionally, time constraints prevented the ninety day aged testing of the BioMed samples. This testing is necessary to gain a better understanding of BioMed's behavior over time. Though the Clear and BioMed resin samples did not perform as hoped, their experimentation led to useful insights into the behavior of the materials and their trends with aging. These results are promising and, hopefully, with future research, they can be used to create the ideal biocompatible bone scaffolding.

Acknowledgements

I would like to thank Sarah López de Armentia, Yolanda Ballesteros, and Eva Jiménez for their invaluable guidance and feedback throughout this research project. Their vast knowledge in this field of study was exceedingly helpful and taught me much regarding material properties and their real world applications. Special thanks should also be given to Eric Johnsen for his oversight and advice on this project. This experience was invaluable and would not have been possible without the support of the Universidad Pontificia Comillas who financed our research.

References

[1] Zhao R, Yang R, Cooper PR, Khurshid Z, Shavandi A, Ratnayake J. Bone Grafts and Substitutes in Dentistry: A Review of Current Trends and Developments. Molecules. 2021 May 18;26(10):3007. doi: 10.3390/molecules26103007. PMID: 34070157; PMCID: PMC8158510.

[2] Paradowska-Stolarz, A.; Wezgowiec, J.; Mikulewicz, M. Comparison of Two Chosen 3D Printing Resins Designed for Orthodontic Use: An In Vitro Study. Materials 2023, 16, 2237. https:// doi.org/10.3390/ma16062237

[3] Lopez de Armentia S, Fernández-Villamarín S, Ballesteros Y, et al., 2022, 3D Printing of a Graphene-Modified Photopolymer Using Stereolithography for Biomedical Applications: A Study of the Polymerization Reaction. Int J Bioprint. http://doi.org/10.18063/ijb.v8i1.503

[4] Bronzoni, Marco. "Impact Charpy." Instron, Instron, 9 Mar. 2022, www.instron.com/en/resources/glossary/charpy.

[5] "Electromechanical Desktop Testing Machine MONOTRAC / DUOTRAC." Ibertest Advanced Testing Solutions, Ibertest, 11 June 2020, www.ibertest.es/products/maquina-de-ensayo-electromecanica-serie-monotrac-duotrac/.

[6] "Clear Resin V5: General Purpose Resin." Formlabs, Formlabs, 20 Mar. 2024, formlabs-media.formlabs.com/datasheets/2401900-TDS-ENUS-0.pdf.

[7] Topsakal K., Aksoy M., Duran G. (2023). The effect of aging on the mechanical properties of 3-dimensional printed biocompatible resin materials used in dental applications: An in vitro study. *American Journal of Orthodontics and Dentofacial Orthopedics, 164*(3), 441-449. https://doi.org/10.1016/j.ajodo.2023.05.023

[8] Formlabs Press. *Form 3 and Wash-Cure*. 21 June 2019. Somerville, MA.

[9] IPC Association Connecting Electronics Industries. (2013). *Test Methods Manual (IPC-TM-650)*. https://www.ipc.org/sites/default/files/test_ methods_docs/2.4.52.pdf

[10] "ISO 178: 3-Point Bend Test on Plastics." *ISO 178 | 3-Point Bend Test on Plastics*, www.zwickroell.com/industries/plastics/thermoplastics-and-thermosetting-molding-materials/3-point-flexure-test-iso-178/. Accessed 5 July 2024.

[11] Hosen, Md. Sarif & Hoque, Md & Rahman, Dr & Suresh, Sagadevan. (2022). Aging Effects on Mechanical Properties of Biocomposites with Recycled Polymers. 10.1007/978-981-16-8360-2_17.

Appendix A: Sample Dimension and Material Type Summary Table

In the duration of this research project, four tests were performed on four different material types and used two different structure builds. To provide clarity into the dimensions of each sample type as well as which tests were carried out on which samples, Table 3 has been detailed below. Note that the "Clear + MMA + NS" material type refers to the Clear resin strengthened with MMA and nanostrength while the "Clear + MMA + dNS" material type refers to this same material formula but with the key difference being that the nanostrength was dried before its integration; the "d" in front of "dNS" denotes this.

Table 3. Sample types and corresponding sample dimensions and materials used with build structure indicated. Spots left blank have no associated dimension or were not printed in the related material.

	Dimensions				**Materials**			
Sample Type	Height (mm)	Width (mm)	Length (mm)	Diameter (mm)	Clear	Clear + MMA + NS	Clear + MMA + dNS	BioMed (Aged)
SENB	7	14	56	-	-	-	Bulk	Bulk
Charpy	4	10	80	-	Bulk	Bulk	Bulk	Bulk & Porous
Bending	4	10	80	-	Bulk	-	Bulk	Bulk & Porous
Compression	12	-	-	6	Bulk	Bulk	Bulk	-

Appendix B: Fracture Toughness Function

To calculate fracture toughness in Eq. (1), a correction factor specific to the geometry was necessary. This correction factor came in the form of the function $f(\frac{a}{W})$ which maps a relationship between a specimen's crack length and overall width. Equation (5), below, elaborates on this function.

$$f(\frac{a}{W}) = \frac{3 \cdot (a/W)^{0.5} \cdot [1.99 - (a/W) \cdot (1 - a/W) \cdot (2.15 - 3.93 \cdot (a/W) + 2.7 \cdot (a/W)^2)]}{2 \cdot (1 + 2 \cdot (a/W)) \cdot (1 - a/W)^{3/2}} \quad (5)$$

Here, a represents the sample's initial pre-crack length while W represents the sample's width, measured in the direction of crack propagation (see Fig. 2). To use Eq. (1), a key assumption was made. The equation itself was based on the principle that the crack would propagate under plane strain conditions. For this to be true, the sample needed to be sufficiently thick, meeting the specimen thickness criterion outline below in Eq. (6).

$$a,\ W > \frac{2.5 \cdot (K_{IC})^2}{\sigma_{YS}^2} \quad (6)$$

In this equation, K_{IC} represents the plane strain fracture toughness while σ_{YS} represents the yield strength. To ensure the validity of the SENB test results, the SENB samples' dimensions were standardized and approved using the thickness criterion from Eq. (6).

Appendix C: Critical Load (P_Q) Data Modeling Example

To determine the fracture toughness of a material, a key variable, P_Q, must be determined. Force and displacement are first plotted against one another, forming the graph seen in Fig. 10(a). The steady state slope of the Force-Displacement curve is then isolated and is pictured in Fig. 10(b).

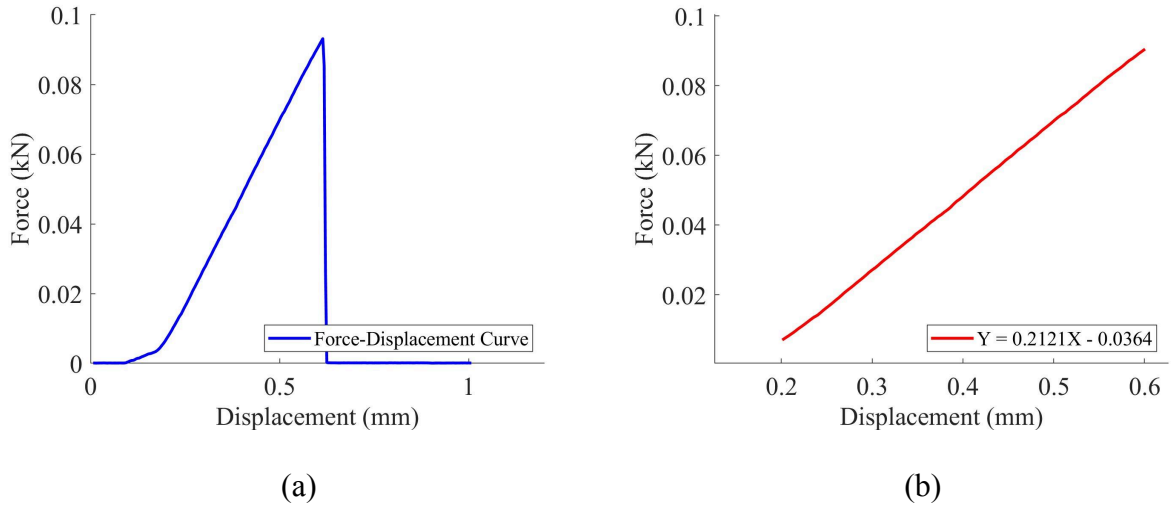


Figure 10. Plots of the Force-Displacement Curve (a) and isolated steady state slope (b). Data for the Force-Displacement Curve was collected following SENB testing. This testing first saw an exponential relationship between force and displacement as the downwards force was initially applied to the sample. The sample soon achieved steady state and experienced regular displacement in the fracture crack opening with the added force; this can be seen in Fig. 10(a)'s constant slope which was isolated in Fig. 10(b). Eventually, the displacement became too great and the sample fractured, causing the sharp decrease seen last in Fig. 10(a).

After isolating the steady state slope, a line with a slope 5% less than the steady state was projected onto the curve. P_Q is then the intersection of this 5% line with the curve or, if the curve reaches a maximum before that point, P_Q is the maximum of the curve. See Fig. 11 for a model.

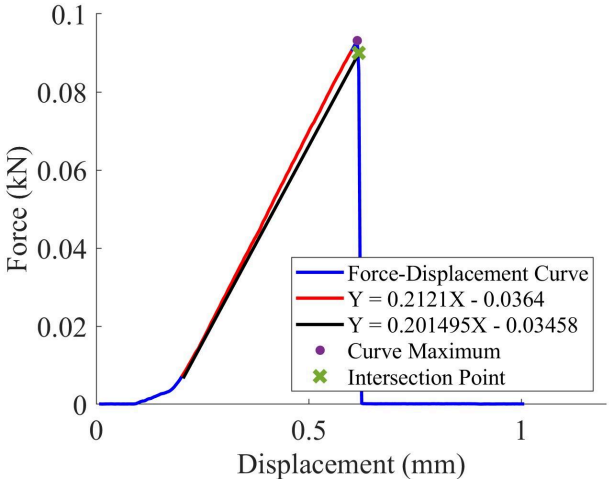


Figure 11. Plot of the 5% steady state slope against the Force-Displacement Curve. The 5% steady state slope is modeled in black while the initial steady state slope is modeled in red and overlaps with the blue Force-Displacement Curve. The curve reaches its maximum force value of 0.0931 kN at a displacement of 0.6145 mm. The 5% line intersects with the curve at a displacement of 0.6177 mm and a force value of 0.0899 kN. Because the curve reaches its maximum force value before the 5% line intersects with it, the P_Q value for this sample would be 0.0931 kN.

Appendix D: Young's Modulus Data Modeling Example

To determine the Young's Modulus for the bending and compression tests, a plot of the sample's stress-strain was first created. The initial slope of the stress-strain curve was calculated and further isolated on a secondary plot. The purpose of this additional graph was to more clearly see the relationship between stress and strain. Ideally, this line would be straight; a curved line would indicate that the data for the Young's Modulus was taken beyond the yield stress. An example of the two graphs used in the Young's Modulus calculations is depicted below in Fig. 12.

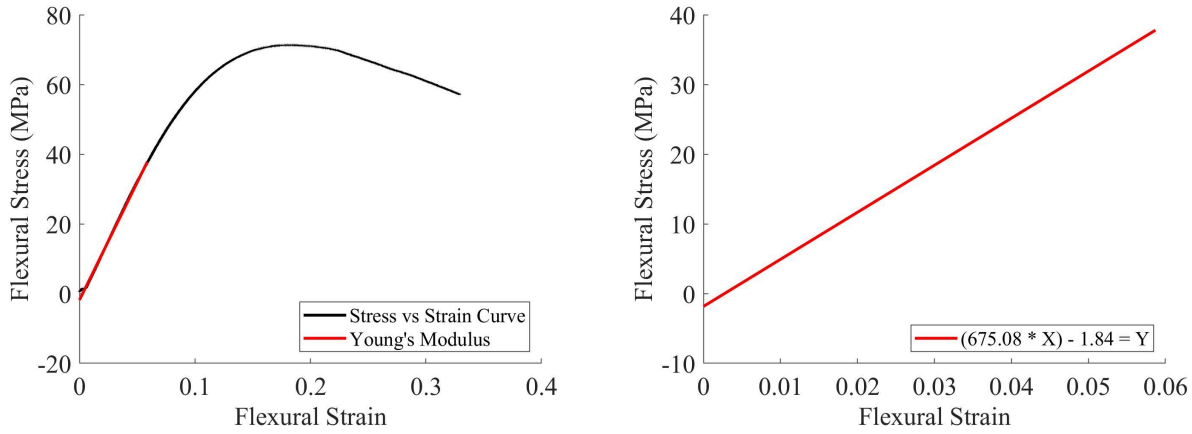


Figure 12. Plots of Stress vs Strain. Figure 12(a) depicts the stress-strain curve with the red line marking the average slope of the initial loading stage. Figure 12(b) isolates this slope. The Young's Modulus here is 675.08 MPa or the average slope of the red line.

To provide further context into the Young's Modulus calculations as well as the stress-strain curve components, Fig. 13 is detailed below. Three key material properties—Yield Strength, Ultimate Tensile Strength, and fracture point— are mapped onto the curve.

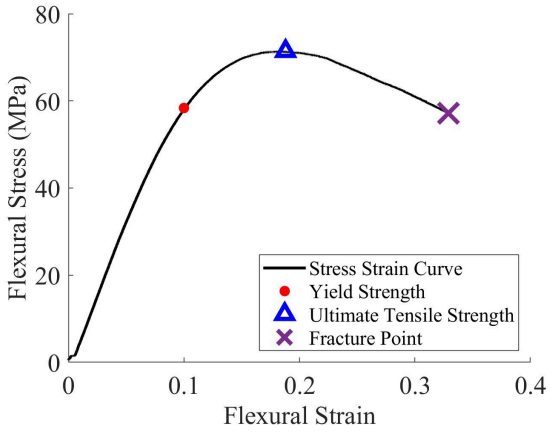


Figure 13. Plot of Stress vs Strain with additional mechanical properties identified along the curve. The red dot along the curve marks the sample's Yield Strength. Yield Strength is the limit at which a material's elastic behavior ends and its plastic behavior begins. In other words, it is the point at which the maximum stress can be applied to the material before permanent deformation. The Ultimate Tensile Strength (UTS), marked by the blue triangle, is a measure of the highest amount of stress a material can withstand while undergoing bending or compression. Lastly, the fracture point, marked by the purple X, is the point at which the material succumbs to the stress and actually breaks.